



Aperture measurements and seepage properties of typical single natural fractures

Wentao Xu¹ · Xiaozhao Li^{1,3} · Yangsong Zhang² · Xiyong Wang⁴ · Richeng Liu³ · Zhicheng He¹ · Jing Fan¹

Received: 2 July 2020 / Accepted: 29 July 2021 / Published online: 18 August 2021
© Springer-Verlag GmbH Germany, part of Springer Nature 2021

Abstract

Fractures play an important role in controlling the hydraulic conductivity of rock masses, and the aperture significantly influences the magnitude of fracture seepage. In this study, field measurements and experiments were conducted at a well-exposed granite fracture site in the Beishan area, China. Several types of single natural fractures were selected to remove the weathered surface and expose the fresh fractures. Subsequently, measuring ruler dispersion-tangent middle axis (MRD-TMA) method was developed to measure the fracture aperture and capture fracture geometry. Then, electrical resistivity tomography (ERT) technique was employed to investigate the seepage properties of these fractures. The results reveal that MRD-TMA method achieved good flexibility and accuracy in the current measurement of fracture aperture, and ERT is a useful tool for detecting the seepage properties of fractures in hard rock masses. Combined with field observations, the filling form of fractures can be categorized according to the ERT inversion results, as follows: open-weak filling, open filling, loose filling, and fully cemented-closed form, whose seepage properties decrease as the filling density increases. Generally, the open-weak filling is the main water channel in a fracture network, while the fully cemented-closed type is a water-blocking fracture and typically exhibits a pseudo-fracture with a large surface opening. In summary, the method for obtaining the morphological characteristics of the aperture can provide a low-cost and time-efficient approach for fracture logging in the field, and ERT technique provides a reference for the detection of potential hazards caused by connected water-conducting fractures in rock engineering.

Keywords Granite fracture · Aperture geometry characteristics · Fracture permeability · Digital image processing · Electrical resistivity tomography

Introduction

The natural fracture network in a rock mass does not only have an important effect on the properties of the rock mass, but is also the main channel for water or solute transport

and storage, which is of interest to oil and gas exploitation, groundwater utilization, environmental remediation activities, and hazardous waste disposal (Yasuhara et al. 2006; Liu et al. 2021; Azimian and Ajalloeian 2015; Baek et al. 2017; Wang et al. 2018; Zhang et al. 2019; Xu et al. 2021). The refined study of single natural fractures in a fracture system is an important foundation for elucidating the characteristics of complex fracture networks, among which the two most critical problems, namely, the aperture characteristics and seepage properties of single fractures, are highlighted. The effective investigation of the two research objectives can clarify the control mechanisms and key parameters of flow and transport in fractured media, and provide an important reference for the implementation of related engineering.

The fracture aperture is the distance between the two fracture surfaces (two contour surfaces) of a fracture in a rock mass. Traditionally, field aperture measurements have been made through the insertion of a feeler gauge (Priest

✉ Xiaozhao Li
lixz@nju.edu.cn

✉ Yangsong Zhang
zhangys@njust.edu.cn

¹ School of Earth Sciences and Engineering, Nanjing University, 163 Xianlin Avenue, Nanjing 210023, China

² Department of Civil Engineering, Nanjing University of Science and Technology, Nanjing 210094, China

³ State Key Laboratory for GeoMechanics and Deep Underground Engineering, China University of Mining and Technology, Xuzhou 221116, China

⁴ Beijing Research Institute of Uranium Geology, Beijing 100029, China

1993). Although this method can achieve a simple opening size value, it does not achieve more accurate geometric features, and the measurement value is vulnerable to the limited measurement accuracy of the feeler gauge. Because the aperture is a very important feature in the study of fracture morphology, a method for accurately capturing the geometric shape of the aperture has been investigated by numerous studies. Brown et al. (1986) established the correlation between the fracture surface and the distribution of the aperture opening degree by considering the digital profiles of the fracture surface. Another destructive measurement method consists of injecting resin or a metal liquid into the fracture aperture to form a cast, and the morphological characteristics of the aperture are obtained after cooling and solidification (Gentier et al. 1989). To promote the systematic study of fracture samples, various nondestructive methods such as transmitted light (Detwiler et al. 1999), spectrophotometric analysis, and magnetic resonance imaging (Renshaw et al. 2000) have been developed to measure the fracture aperture. More effectively, the X-ray computed tomography (CT) technique has been employed to obtain refined measurements of microscale fracture apertures (Geet and Swennen 2001; Mazumder et al. 2006; Schlüter et al. 2014; Ramandi et al. 2016; Huo et al. 2016; Ketcham and Mote 2019). The CT imaging method provides high-precision technical support for the measurement of the fracture opening and can provide an accurate description of the fracture aperture geometry, which is however limited to microscale samples and restricted to laboratory measurements. At some engineering sites, geological engineers are required to catalog the fractures in a timely manner, but sampling each fracture for laboratory CT imaging measurements is impractical. Therefore, it is imperative to develop techniques for rapid and efficient field fracture measurements with wide applicability. In the field of civil engineering, image processing technology is widely used for fracture recognition and detection (Yu et al. 2007; Montero et al. 2017; Li et al. 2020). In this regard, using a high-resolution Charged Couple Device camera is an effective method for achieving the engineering accuracy, and accurate image calibration is a key step in fracture detection (Ali et al. 2014). However, these methods are only used to detect the fracture distribution, and cannot determine the fracture width. In fact, owing to the roughness and complexity of rock fractures, the accurate measurement of the fracture aperture is challenging, particularly under in-situ conditions.

The flow characteristics of fracture networks in rock mass, and particularly in crystalline rocks, depend on the flow characteristics of a single fracture. Presently, single fracture permeability studies are mainly carried out through laboratory sample tests and simulations based on the obtained geometry of the sample aperture (Xiong et al.

2011; Zhang et al. 2015; Ramandi et al. 2017; Hooker et al. 2013; Karimpouli et al. 2017; Huang et al. 2019; Wu et al. 2020). In these studies, fractures are idealized as having good hydraulic conductivity. However, based on field investigations, Xu et al. (2019) conducted a simulation and concluded that the permeability of a fracture network consisting of single fractures differs by 4 orders of magnitude, regardless of whether the fracture aperture is partially filled or not. Therefore, more attention should be paid to the seepage of natural fractures in the field, so as to make relevant lab tests and simulations more reasonable by considering the flow properties of actual natural fractures. Therefore, challenges in capturing the fracture flow properties in a rock mass under in-situ conditions are highlighted. The electrical resistivity tomography (ERT) technique is a non-conventional geophysical method and provides a potentially feasible approach toward obtaining the hydraulic conductivity of fractures in rocks, because this technique is widely used to detect the internal environment and related characteristics of water bearing media (Bharti et al. 2021; Hoorde et al. 2017). Based on soil resistivity characteristics, which change with the water content, Zhou et al. (2001) used the ERT technique to monitor the three-dimensional spatial-temporal variation of soil water content and demonstrated the potential of ERT for use in the monitoring of porous water bearing media. At the Krauthausen test site in Germany, Kemna et al. (2002) successfully captured the flow characteristics of solute transport in an underground aquifer using the ERT technique, and concluded that ERT can effectively quantify the variability of parameters relevant to flow and transport in heterogeneous aquifers. Inspired by the application of the ERT technique to porous media and aquifer media, the effectiveness of the ERT technique in investigating the hydraulic conductivity of different types of fractures in crystalline rock should be evaluated.

To investigate the geometrical characteristics of typical natural fractures under in situ conditions and their corresponding seepage properties, based on the authors' previous research, a well-exposed granite fracture outcrop in the Beishan area of China was selected to establish a three-dimensional (3D) point cloud model. Fracture dominant grouping was performed using the method proposed by Xu et al. (2020). Combined with field investigation, several single fractures with typical characteristics were selected, and the surface area affected by weathering was cut away and polished to expose the smooth and flat fresh fracture surface. The measuring ruler dispersion-tangent middle axis method is proposed to digitally measure the fracture aperture size, and the characterization and geometric characteristics of the fracture aperture are discussed. To understand the seepage properties of fractures with different filling

forms, the ERT technique was employed to characterize and infer the seepage of the fracture media by adding salt water. The obtained results are discussed and analyzed in light of field observations.

Preparation of typical fractures

The study area is located at the Xinchang site in the Beishan area (Gansu Province, Northwest China), which has been selected as a candidate site for the Chinese underground research laboratory built for a high-level radioactive waste repository (Chen et al. 2015; Wang et al. 2018). Here, through geophysical investigation, the geological structure has been determined to be mainly granite with single lithology (Wang 2010). Owing to the characteristics of granite itself and other geological processes, a large number of natural fractures exist in the granite body (Fig. 1). Natural single fractures crisscross to form complex fracture networks, which directly affect the rock mass characteristics.

Selection of typical fractures

Through a large number of geological field investigations, it has been found that the fractures exposed at this site do not have a completely random distribution, but instead certain clustering characteristics. In other words, these fractures can be divided into different dominant sets according to their orientation characteristics (Guo et al. 2015; Wang et al. 2018; Xu et al. 2019, 2020). The use of this method promotes the modeling of fracture networks, and the characteristics of single fracture have a crucial impact on the fracture network. Therefore, a typical fracture outcrop was



Fig. 1 Complex fracture networks formed by crisscross single fractures

selected to investigate the two most important characteristics of a single fracture in a fracture network, namely, the geometric and permeability characteristics. First, the 3D reconstruction model of the outcrop was obtained by photogrammetry modeling. Thus, the exposed fractures were identified and extracted. Then, the outcrop fractures were divided into four dominant sets depending on the orientation characteristics (Fig. 2). The specific implementation method used in this study was proposed by Xu et al. (2020). According to the dominant grouping results, four typical fractures were selected through field observation. Area Y_{1-1} was selected for the first investigated fracture type, and the color of the model is green. Area Y_{1-2} was mainly used to investigate the second fracture type, and the color of the model is red. Area Y_{1-3} belongs to the third typical fracture, and the color of the model is blue. Area Y_{1-4} belongs to the fourth type, and the color of the model is pink (Fig. 2). Among them, fracture Y_{1-1} represents the open-weak filling type, fracture Y_{1-2} represents the open filling type, fracture Y_{1-3} represents the fully filled-cemented type except the surface opening, and fracture Y_{1-4} represents the loose filling type. The four different fracture types considered here are only presented to analyze the relevant characteristics of fresh fracture surfaces, and the influence of the weathering grade on the surface is not considered. Therefore, readers interested in the details of the identification and categorization of the weathering grade in granite exposures should refer to the relevant literature (Singh and Basu 2018; Basu et al. 2009).

Acquisition of fresh fracture surface

Through the field survey, it was found that although the fractures on the exposed surface were adequately developed, the actual information of the aperture opening was lost as a result of weathering (Fig. 3a). The typical features observed in the surface fractures are relatively broken or loose false fractures with an increased opening degree, which is detrimental to any results obtained only by surface investigation. The so-called false fracture (or pseudo-fracture) refers to a kind of fracture whose surface opening degree has significant change compared with the original fracture opening due to weathering and other reasons. Therefore, we tried to cut and polish the selected typical fractures in the research area in situ using a cutting machine and grinder to expose the fresh fracture surface. The rock surface was first cut by a rock cutter to form crisscross small pieces (Fig. 3b). After removing these pieces, the exposed fracture surfaces were polished with an angle grinder to form a flat fresh surface (Fig. 3c). Since the granite outcrop in the study area belongs to hard rock, weathering only causes significant changes in the surface opening, so in order to ensure that the aperture opening of fresh fractures can be measured, the preparation

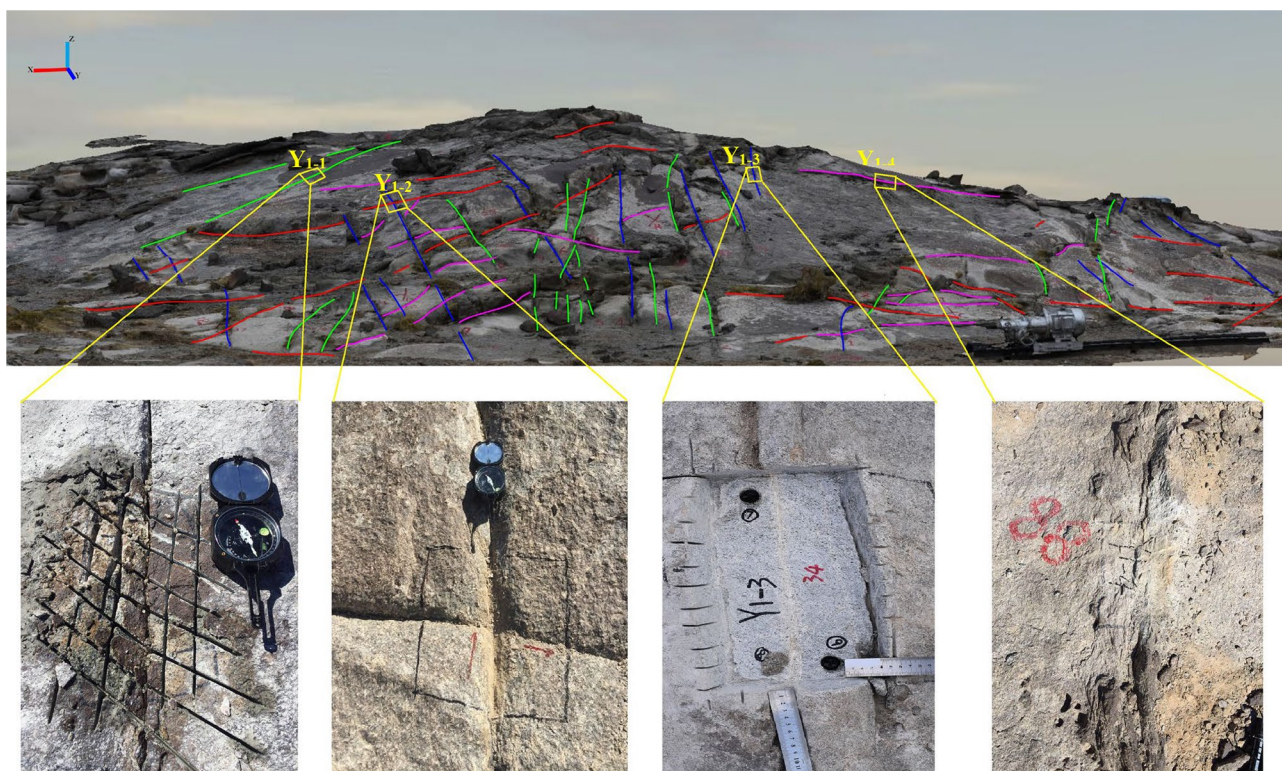


Fig. 2 Dominant grouping of granite outcrop fractures and selection of typical characteristic fractures

process for obtaining fresh fracture surface is performed by cutting 5 cm downward. Notably, granite is very hard and special attention should be paid to safety during the implementation of the above-mentioned process.

Methodology and experimental design

Equipment

The objective of this study was to investigate the geometrical characteristics and permeability properties of fractures. Therefore, a high-resolution camera (Nikon-D750) with a F35-mm fixed focal length lens was employed to capture

high-resolution pictures of the fractures. This camera can capture pictures with up to 24 million effective pixels, and has a good photosensitive system. Additionally, a network parallel electrical exploration instrument (NPEI-DHZI-1) with high-resolution measurement accuracy and sensitivity was used to investigate the connectivity and water conduction characteristics of the fractures. The measurement current resolution of this device has an accuracy of $1 \mu\text{A}$, and is very sensitive to the electrical conductivity of the target medium. Generally, the sampling time is 0.5 s, and the interval time is 50 ms, which can ensure the accuracy of the field test results. Moreover, a high-precision straight steel ruler was used as a reference scale for the fractures in the captured photos, a millimeter feeler gauge was used to



Fig. 3 Exposure of fresh fracture surface by removing the influence range of surface weathering in research area. (a) Weathered fracture surface. (b) Process of removing the weathered fracture surface using cutting machine. (c) Exposed fresh fracture surface using grinder machine

measure fractures with obvious openings, and measuring tape was used to measure the fracture length.

Aperture measurement

In the acquisition of the fractures' geometric features, the captured high-precision photographs were used to measure the fracture opening degree. The first step was to calibrate the captured photos and obtain an unbiased and distorted standard image. The second stage was to extract the effective fracture area using digital image processing technology. The third stage was to use the tangent center axis method combined with the discrete standard scale value of the steel ruler to calculate the precise fracture aperture value.

Photo calibration and correction

The photos captured on site are two-dimensional. Owing to the angle deviation and lens distortion of the camera, the photos were deformed to a certain extent compared with the actual objects. Particularly, the angle deviation at the edge of the photo led to inaccurate information. The effective part of the photo is typically captured during the digital measurement of the aperture. Therefore, the orthophoto method of angle correction was adopted to correct the captured photos. The orthophoto correction of the image is based on the perspective principle to perform the center projection transformation of the image.

Assuming that the central light source is point S , to simplify the derivation, vertex p_{00} and q_{00} of the two quadrilaterals are coincident and uniformly represented by O . p is a point in the quadrilateral, and q is the corresponding point of p in the rectangle (Fig. 4). According to the principle of center projection transformation, the formula of shadow transformation can be written as follows:

$$(x_0, x_1) = \frac{(a_1 \cdot (a_0 + a_1 - 1) \cdot y_0, a_0 \cdot (a_0 + a_1 - 1) \cdot y_1)}{a_0 \cdot a_1 + a_1 \cdot (a_1 - 1) \cdot y_0 + a_0 \cdot (a_0 - 1) \cdot y_1} \quad (1)$$

where (x_0, x_1) are the coordinates of the inner points of the rectangle, and (y_0, y_1) are the quadrilateral coordinates of the inner points of the rectangle. a_0 and a_1 , which are constructed as the solution of two linear equations, are two coefficient constants.

This equation indicates the one-to-one mapping relationship between the pixel coordinates of the new graph and the pixel coordinates of the source graph. Then, the pixel points of the new graph are assigned by the most domain interpolation to obtain the corrected image.

It should be noted that in the actual shooting process in the field, the best focal length should be adjusted to make the fracture photos clear and shoot the fracture as perpendicular to the shooting direction as possible. In this way, the

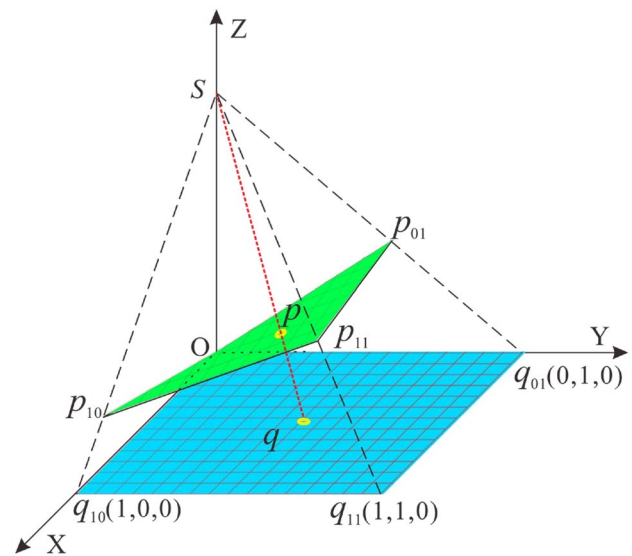


Fig. 4 Photo angle correction and center projection transformation diagram

angle deviation and lens distortion can be ignored, so as to improve the accuracy of fracture measurement.

Digital image processing for fracture area

The original image containing substantial hue information (RGB) does not facilitate the calculation and processing of fractures (Fig. 5a). Therefore, an appropriate threshold was selected according to the grayscale histogram of the original image. If the gray value of the original image was greater than the threshold value, the gray value returned to 255 (white). For the part that was below this threshold, the gray value returned to zero (black). The image obtained after gray processing is shown in Fig. 5b. Because the photo shown in Fig. 5b contains a large amount of noise, the image contrast was enhanced through gray scale transformation and mapping, and then the isolated noise point was eliminated using median filter without reducing the contrast of the image (Fig. 5c). The maximum inter-class variance method (Otsu's method) was used to segment the image and reconstruct the gray image. Then, the threshold transformation method was employed to convert the gray image into a binary image (Fig. 5d). The shape of the fracture can be clearly seen through the binary image, but some noise still existed in the image and affected the automatic calculation. Severe noise can erroneously segment a fracture into several small fractures. Therefore, the black noise inside the fracture was filled using binary image hole filling technology, and the white noise in the non-fracture area was deleted. The effective fracture area was selected using the morphological method as shown in Fig. 5e. Finally, the image was corroded

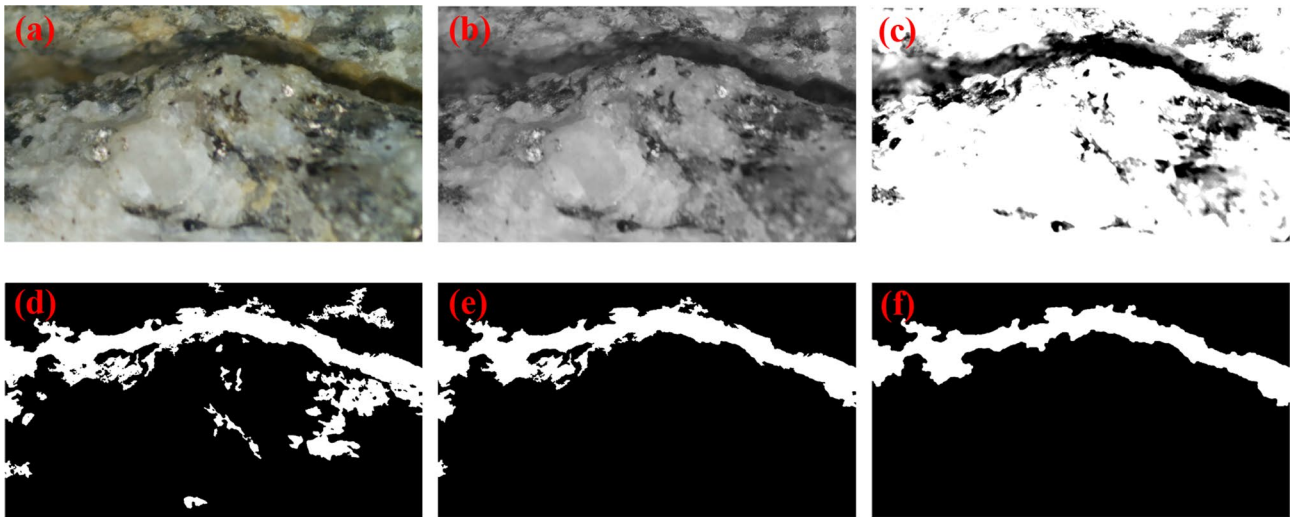


Fig. 5 Image processing for fracture area. (a) The original picture/image, (b) Grayscale image, (c) Image enhancing and filtering, (d) binary reconstruction image, (e) micro processing of binary noise, and (f) smoothing of binary image

$(A \ominus B)$ and expanded $(A \oplus B)$. A corresponding closing operation was performed to eliminate the burr and bumps on the fracture boundary, and to bridge the small disconnection and obtain a smooth fracture contour (Fig. 5f).

Tangent middle axis measurement algorithm

Considering the shortcomings of traditional methods, this section proposes the tangent middle axis algorithm for aperture measurement based on the improved polygon centroid. The fracture can be considered a polygon within a small range; therefore, the medial axis of the fracture comprises a series of continuous medial points along the length of the fracture in

a zig-zag shape (Fig. 6). Figure 6 shows the upper and lower boundaries of the fracture contour extracted from Fig. 5d.

Owing to the irregularity of the fractures, there may be more than one pixel in a column i . Therefore, optimization should be carried out such that the corrected fracture medial axis is only one pixel wide.

$$M(i) = \frac{\sum_{k=1}^{L(i)} F(i, k)}{L(i)} \tag{2}$$

where $(i, M(i))$ is the new medial axis point of column i and $(i, F(i, k))$ represents all pixel coordinates in the fracture region of the i th column. $L(i)$ is the number of fracture pixel points in column i .

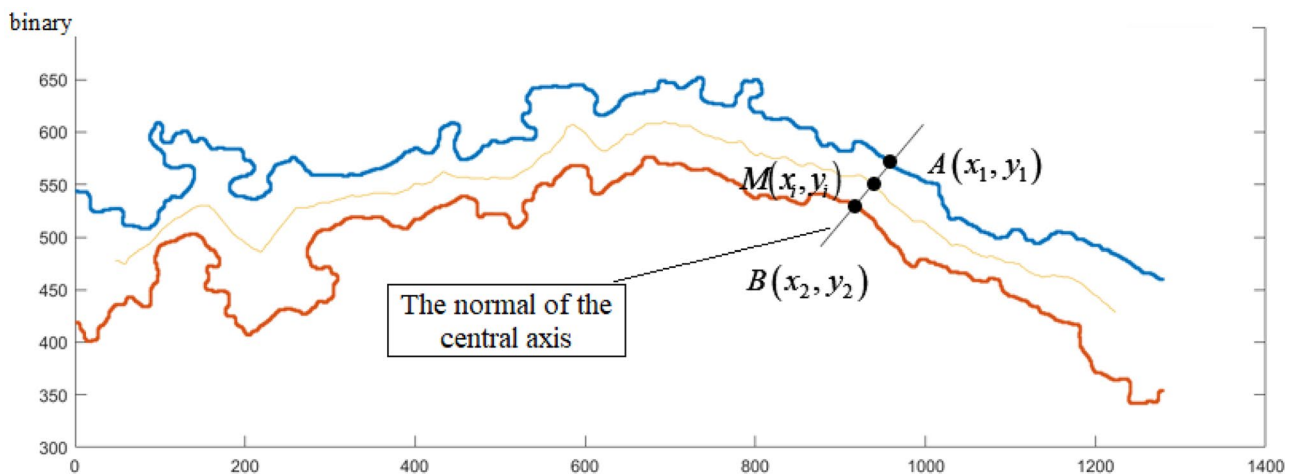


Fig. 6 Schematic diagram of obtaining the fracture opening of the tangent middle axis

Therefore, the normal equation at the medial axis point i can be expressed as follows:

$$f(x) = -\frac{1}{C(i)}(x - i) + M(i) \quad (3)$$

where $C'(i)$ is the slope of the tangent line at point $(i, M(i))$. To accurately reflect the tangent line of the medial axis at point $(i, M(i))$ and ensure the stability of the slope calculation of the tangent line, n pairs of medial axis coordinates close to the point i were selected to calculate the slope of the point, and the average value of n slopes was the tangent line slope of the medial axis at point i .

$$\bar{C}(i) = \frac{M(i+n) - M(i-n)}{2n} \quad (4)$$

When the tangent slope value $\bar{C}(i)$ is zero, the normal line of the medial axis is a vertical segment, which indicates that the corresponding fracture aperture at this point is the difference between the vertical coordinates of the upper and lower boundary of the fracture.

Furthermore, owing to the complex upper and lower boundary morphology of the fractures, it is difficult to obtain the expression of the boundary function. Therefore, the “making difference” method was adopted to determine the upper boundary intersection point $(x_1, U(x_1))$ and the lower boundary intersection point $(x_2, L(x_2))$. To satisfy the calculation accuracy requirements, the two obtained boundary points should meet the following expression:

$$|f(x) - B(x)| < \varepsilon \quad (5)$$

where $f(x)$ is the ordinate of the intersection of the medial axis and the boundaries, $B(x)$ represents the boundary point $U(x)$ or $L(x)$, and ε denotes the precision threshold. Here, ε is 1 pixel.

Thus, the fracture aperture corresponding to the medial axis point can be obtained as follows:

$$\text{ape} = \sqrt{(x_2 - x_1)^2 + (y_2 - y_1)^2} \quad (6)$$

Notably, the fracture opening degree value obtained by the above-mentioned method is a pixel value; that is, the image point is used to represent the fracture opening degree. Hence, it is necessary to use an effective method to convert the fracture opening degree into the expression form of a universal unit without being affected by the capture conditions of the camera. Consequently, only a straight steel ruler with an accurate scale is needed. When capturing photos of a fracture, a steel ruler is placed parallel to the fracture strike, and the fracture and steel ruler are captured in the same photograph. After the unbiased correction of the photo using the method described in “Photo calibration and correction,” the scale is separated from the photo, and the fixed length segment in the scale is selected to determine the length

represented by the unit image point. Then, the opening degree of the fracture can be calculated according to the number of image points obtained using the tangent middle axis method. The method of the measuring ruler dispersion-tangent middle axis is very convenient for conducting geological field surveys, and can satisfy the requirement for high precision.

Electrical resistivity tomography technique

Technical principle and inversion method

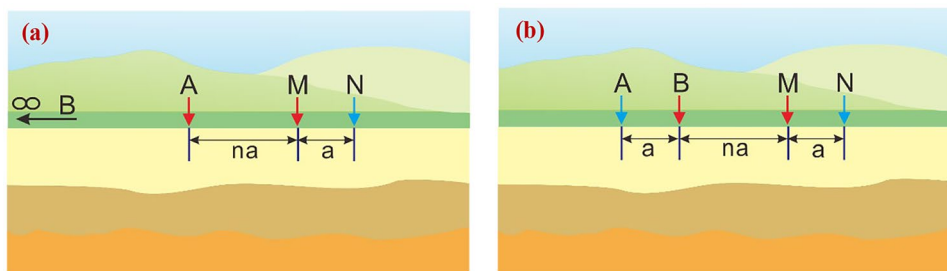
The electrical resistivity tomography technique is a geophysical investigation method. Based on the conductivity difference of the measured media, such as rock and soil, the distribution law of the underground conduction current can be investigated by artificially applying a stable direct current field. Finally, the physical structure characteristics of the detection medium are revealed in the form of a profile. The ERT technique has the advantages of being convenient and intuitive for the perceptual understanding of the characteristics of complex geological bodies (Bellanova et al. 2018; Ravindran et al. 2016). In this study, the network parallel electrical method was used. The basic principle of this method is very simple and identical to that of the conventional resistivity method. For a pair of electrodes A-B arranged on the detection object, a stable current field is formed in the monitoring object by inputting the direct current with strength I through the power supply. The resistivity of the monitoring section can be calculated by measuring the voltage U_M and U_N between the other two arranged metal electrodes M-N. By constantly changing the medium environment in the monitoring object, the change of the resistivity can be comprehensively obtained and then the relevant characteristics of the monitoring objects are reversed as follows:

$$\rho_s = K \cdot \frac{U_M - U_N}{I} \quad (7)$$

where K is a constant related to the layout. ρ_s is the resistivity, which is essentially only related to the environmental medium of the monitoring object.

In the field experiment, the WBDpro electrical equipment was used to collect real-time dynamic data. Then, the raw data were preprocessed to generate the apparent resistivity files and related inversion format files. The widely used EarthImager2D (Nijland et al. 2010) or Res2DINV software (Loke and Barker 1995) can be employed to carry out the two-dimensional or three-dimensional inversion calculation of the physical features. In these approaches, the finite-difference method and the optimized least squares method are used to minimize the mismatch between the measured resistance and the theoretical resistance, and ensure the smoothness of the resistivity image.

Fig. 7 High precision electric method experimental electrode layout. **(a)** Pole-dipole scheme (AM method). **(b)** Dipole-dipole scheme (ABM method)

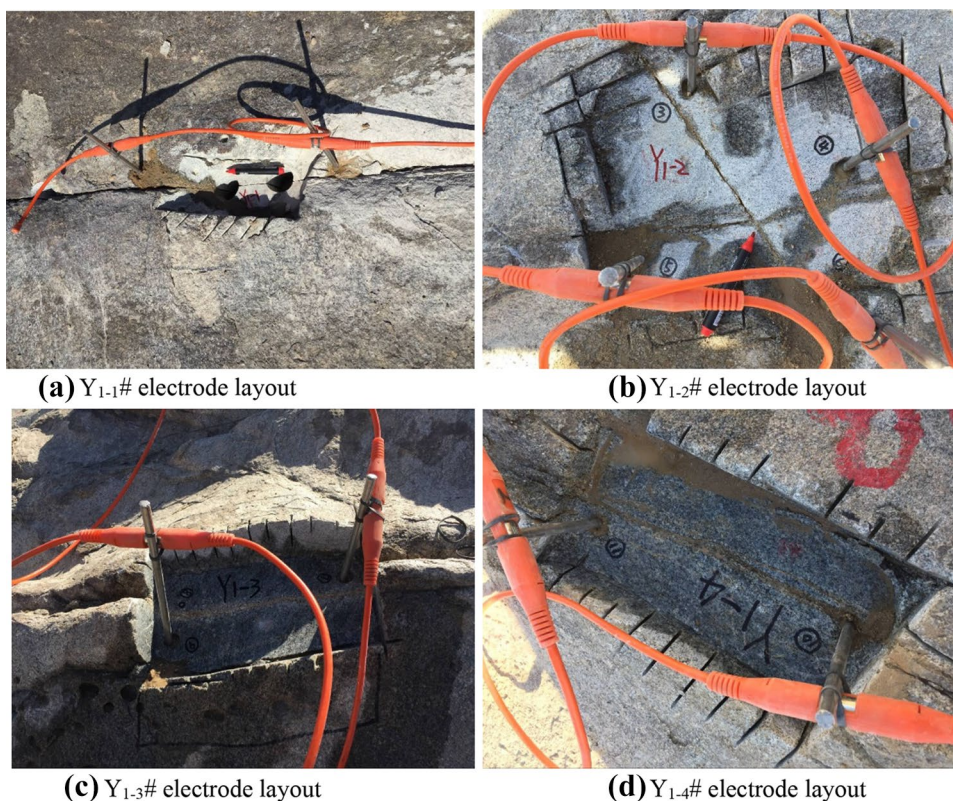


Electrode layout scheme

The electrode layout scheme of the ERT method is sensitive to the inversion results of the detection medium; therefore, it is very important to select an appropriate layout scheme accordance with the target body in the detection. Currently, the most basic and commonly used layout schemes are as follows: Wenner scheme, Wenner-Schlumberger scheme, pole-dipole scheme, and dipole-dipole scheme. Because the experiment conducted in this study was aimed at the seepage of a single fracture, high precision and experimental efficiency are required. Hence, two types of unipolar power supply (three-stage AM method; Fig. 7a) and dipole power supply (ABM method; Fig. 7b) were adopted. In terms of the two layout schemes, the AM method has high measurement efficiency, while the ABM method has high measurement accuracy.

Notably, in the field electrode layout, the depth of the hole inserted into the electrode should not exceed the electrode length. To ensure that the measuring electrode has good conductivity, 30-cm-long stainless steel rods with good conductivity were selected as the electrodes. Based on the selected typical fractures discussed in “Selection of typical fractures,” small holes with depth of 20 cm were drilled according to the fracture orientation. After drilling, the hole depth and hole spacing were recorded in a timely manner and the hole’s serial number was marked. Rubber bands were firmly fastened at the metal electrode junction to avoid the instability of the current field applied to the rock mass owing to the poor contact at the contact point during the test. One end of the electrode was energized, and the other end was placed 200 m away from the test site (infinity). For the single fracture Y_{1-1} , two electrodes were used (Fig. 8a). Because

Fig. 8 Layout of several typical fractures resistivity imaging electrodes. **(a)** Y_{1-1} # electrode layout. **(b)** Y_{1-2} # electrode layout. **(c)** Y_{1-3} # electrode layout. **(d)** Y_{1-4} # electrode layout



the two fractures intersected in region Y_{1-2} , the four electrodes were used to measure the seepage properties (Fig. 8b). Similarly, the single fractures Y_{1-3} (Fig. 8c) and Y_{1-4} (Fig. 8d) were measured using two electrodes, respectively.

Test procedures

To promote the conductivity of the medium, saline water with a certain concentration was prepared (the concentration of Na⁺ in the salt solubility was approximately 1200 mg/L). The specific experimental steps were divided into two parts, namely, the initial measurement and the measurement after adding the salt solution. First, the power supply was turned on, and the initial test (dry test) was performed to obtain the initial values between the electrodes after the current and voltage were stabilized. The initial values were recorded and stored in a timely manner. Next, the prepared saline water was injected into the borehole containing the electrode (the injection volume was 100 ml). After 15 min, the seepage was essentially stable, and the second test (wet test) was conducted. Then the next measurement was carried out in turn. The measurement began 15 min after each addition of saline water, and the wet measurement was performed for five times for each fracture. The connectivity of the test area and the seepage of each tested fracture were qualitatively obtained through the interpretation and inversion of the acquired original data. Notably, the time interval for the measurement should be more specific to the resistivity curve reflected by the electrical equipment, and should be determined according to different environmental conditions. The measurement time should not be too early,

because the solution will have not diffused at this time, nor too late, because the solution flow will have been completed.

Results and analysis

Validation of measurement method

Generally, to conveniently measure and calculate the fracture opening in a binary image, the fractures in the binary image are divided into several small segments and each segment is used as an independent object for fitting (Fernelund 2005; Zhang et al. 2012; Banerjee et al. 2019). The circle diameter, the axial length of the ellipse, and side length of the rectangle obtained after fitting are used to represent the width of the segment fracture, which corresponds to the equivalent area circle, equivalent area ellipse, and minimum enclosing rectangle method, respectively (Fig. 9a). According to the area rule, the corresponding width of the segment can be obtained, and then the distribution of the fracture aperture along the length direction can be captured (Wang 2006). Although the operation of these methods is simple, the measurement accuracy largely depends on the width of the fracture segment division and the fracture morphology. Additionally, in the traditional centerline method, the sum of the shortest distance from the point on the medial axis to the upper and lower boundaries is the fracture aperture corresponding to the point. This method has strict requirements with regard to the fracture morphology. When a fracture boundary is complex and its change gradient is large, the accuracy of the fracture boundary will be reduced.

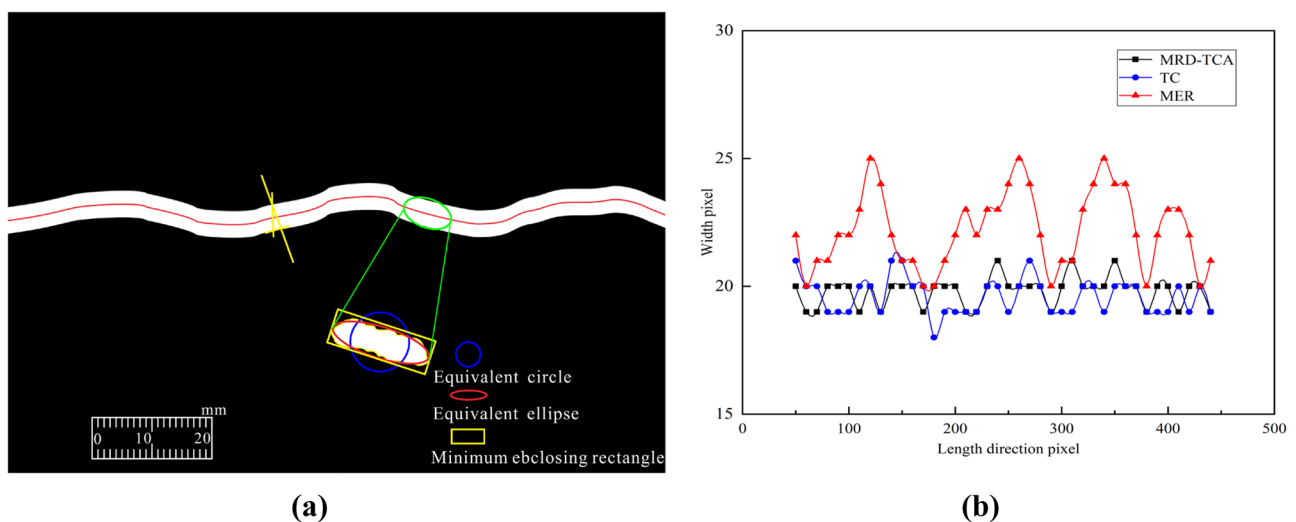


Fig. 9 Schematic representation of fracture and obtained results of aperture using various methods. (a) the ideal fracture with constant width of 20 pixels and the principles of several measurement techniques; (b) results obtained using different methods

Table 1 Ideal fracture measurement results using different methods

Measurement method	Average opening value (pixel)	Standard deviation	Relative error	Frequency of the truth value	Measurement value (mm)
TC	19.59	0.7089	2.1%	17	3.92
MER	22.21	1.5055	11.1%	6	4.44
MRD-TCA	19.81	0.5639	1.0%	26	3.96

To investigate the applicability of the measuring ruler dispersion-tangent middle axis (MRD-TMA) method to the accurate measurement of the aperture, an ideal fracture with a constant opening of 20 pixels was artificially designed in a 500×350 pixel picture (corresponding to the standard area of 100×70 mm²). By avoiding the influence of the fracture division width, the fracture aperture from the 50th pixel to the 450th pixel was measured using the minimum external rectangle (MER) method, traditional centerline (TC) method, and MRD-TMA method, respectively. The measurement interval was 10 pixels. The measurement results for the designed fracture obtained by the different above-mentioned methods are presented in Fig. 9b and Table 1.

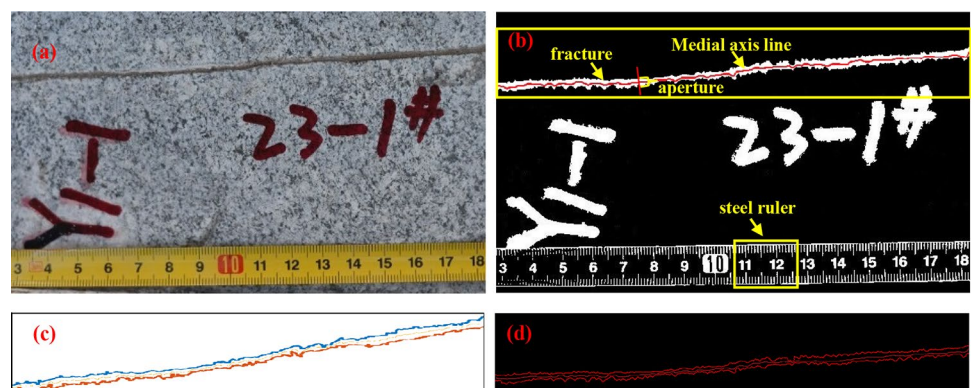
As presented in Table 1, the measurement results of the MRD-TCA method and TC method are essentially the same, and both are close to the actual aperture value of 4 mm. Overall, the measurement results of the MER method exceed the actual value (Fig. 9b). The average fracture aperture is 22.21 pixels (4.44 mm) with a relative error of 11.1% compared with the true value. Furthermore, compared with the TC method, the relative error of the measurement results obtained by the MRD-TCA method is approximately 1%, and the standard deviation is even smaller. The measurement results obtained by the proposed method are equal to the true value with higher frequency, which indicates that the tangent middle axis method for fracture aperture measurement is more accurate and reliable.

Application of aperture measurement method

By considering fracture Y1-1 as an example, the proposed MRD-TCA method was used to accurately measure the fracture opening, and the geometric characteristics of the fracture aperture on the fresh surface were obtained. For the captured photo of fracture Y_{1-1} , the method described in Section "Photo calibration and correction" was adopted to correct the angle deviation (Fig. 10a). The method described in "Digital image processing for fracture area" was employed to achieve the binarization of the fracture image, as shown in Fig. 10b. Notably, the ruler should be sharp to achieve binarization. The fracture medial axis was obtained using the tangent middle axis measurement algorithm described in "Tangent middle axis measurement algorithm" as shown in Fig. 10b and c. Additionally, the Canny operator was employed to extract the skeleton of the fracture region (Fig. 10d). The advantages of using the tangent middle axis method are highlighted by its comparison to other methods.

Figure 10c and d shows that the image processing method used in this study to obtain the fractures has good applicability and can more realistically obtain the fracture edges compared with the widely used Canny operator. Through the above digital processing of the fracture image, the corresponding aperture pixel values were obtained by measuring every 10 pixels along the central axis. Subsequently, the measuring ruler dispersion method was used to determine the size of an image point after binarization. The image can be separated without distortion using angle correction and

Fig. 10 Skeleton extraction and digital measurement of fracture aperture. (a) Original image of fracture and steel ruler after deviation correction; (b) image binarization for fracture and steel ruler; (c) fracture edge and medial axis obtained by tangent middle axis method; (d) the skeleton of the fracture region extracted using Canny operator



pixel calibration; that is, the size of each pixel point on the separated scale is consistent with the size of the pixel point represented on the fracture. Therefore, the 2-cm length of the scale in Fig. 10b was selected for discretization and the size of each unit image pixel was 0.238 mm, which is obviously more accurate compared with the contact measurement method. For the digital measurement results of fracture Y_{1-1} , the maximum value is 2.375 mm and the average value is 1.665 mm. The distribution characteristics of the aperture opening are shown in Fig. 11a. However, the maximum aperture value of the fracture in the field measurement made by a millimeter feeler gauge is approximately 2.1–2.4 mm, which is similar to the result of the digital photo calculation. Thus, it is concluded that the image refinement recognition calculation has good reliability and can greatly reduce the field workload while improving the calculation accuracy.

Furthermore, the aperture distribution characteristics of fracture Y_{1-1} were fitted by several common aperture distribution forms, such as the normal distribution, lognormal distribution, gamma distribution, and generalized extreme value (GEV) distribution. Thus, it was concluded that there is no significant difference among these fitting characteristic curves. To determine the optimal fitting curve of the aperture distribution, the Kolmogorov–Smirnov (K-S) test was carried out to quantitatively analyze the fitting effect. The results of the K-S test for different distributions are reported in Table 2. Because the test values of the null hypothesis H are all zero, the four above-mentioned probability distributions are valid with regard to the distribution characteristics of the fracture aperture. However, the GEV distribution has the largest P value (0.2494) and the smallest K-S value (0.0879), which indicates that the GEV distribution is the best distribution form for the measured aperture.

To investigate the variation of the aperture features within a local scope and in a specific direction, that is, the correlation and randomness of the regional spatial variation characteristics, based on the obtained aperture distribution characteristics, the variation function was used to analyze the

Table 2 The results of K-S test for different probability distribution functions*

Probability distribution function	Kolmogorov–Smirnov test			
	Null hypothesis test result H	P -value	K-S statistics	Critical value
Normal	0	0.2355	0.0773	0.1056
Lognormal	0	0.0625	0.1131	0.1056
Gamma	0	0.1015	0.1011	0.1056
GEV	0	0.2494	0.0879	0.1056

P value > 0.05 indicates acceptance of the null hypothesis

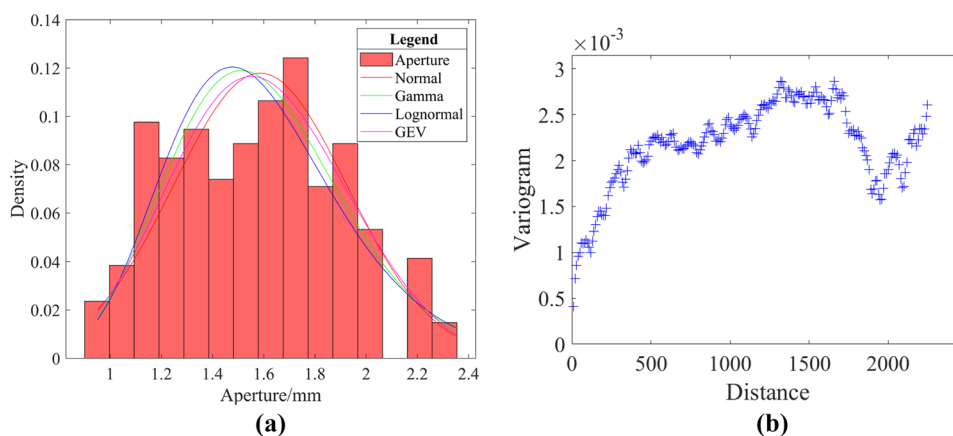
*H=0 indicates acceptance of the null hypothesis

structural variation features of the aperture and the results are presented in Fig. 11b. For the overall variation curve of the selected typical section, at the level of millimeter length, the correlation of the fracture aperture is relatively high, and the experimental variation curve has a nested structure, which indicates a certain scale effect. Based on the analysis of the aperture characteristics of this typical fracture, a large number of samples will be comprehensively analyzed in the future to further investigate the essential characteristics of natural fractures. Additionally, the acquisition of the fracture characteristics will promote the fracture modeling in the laboratory to replace existing completely random simulations.

Analysis of fracture seepage characteristics

The ERT measurements were made at four sites located on a typical granite outcrop to determine the connectivity and hydraulic conductivity of fractures with different characteristics. The relatively low resistivity contrast between the fracture with good water conductivity and the fracture without water conductivity after adding salt solution opened the way to extract water conductivity information of the granite

Fig. 11 Statistical histogram of the aperture distribution and analysis of variation characteristics. (a) Histogram of the aperture distribution and distribution feature fitting. (b) Analysis of variation characteristics of the aperture

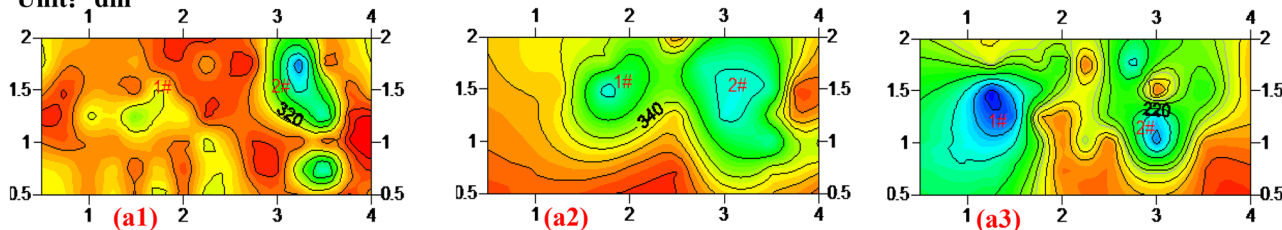


fractures from geophysical investigations. For each site fracture, the inversion profile of the resistivity change characteristics in the medium with the addition of salt water is shown in Fig. 12. Notably, for each group of tests, the initial (measurement without adding any salt water), the intermediate process (measurement with the addition of 300 ml of salt water), and last test (measurement with the addition of 500 ml of salt water) were selected for inversion analysis.

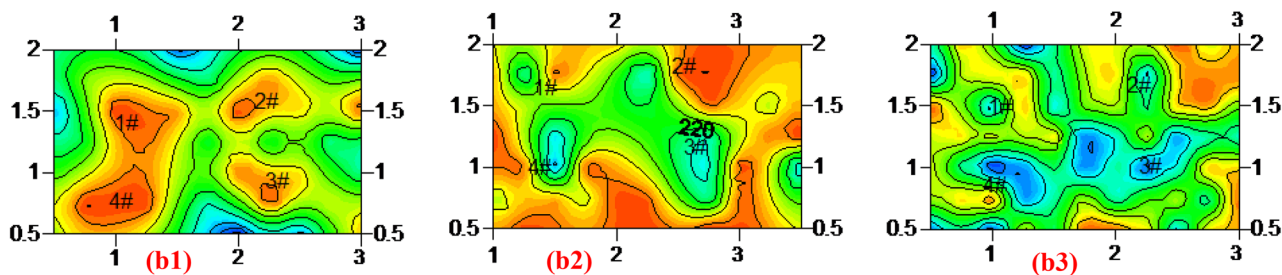
With regard to fracture Y_{1-1} , the initial resistivity was low (approximately $-55 \Omega\text{-m}$) because there was rainwater in electrode hole 2# before the addition of salt water (Fig. 12a1). When salt water was added to electrode hole 2#, the overall resistivity decreased from approximately $500 \Omega\text{-m}$ to $40\text{--}50 \Omega\text{-m}$ after a certain period of time (as shown in Fig. 12a2). When the last water addition was completed, it can be seen that the resistivity at electrode 1# was extremely low,

(1) Fracture Y_{1-1} test results.

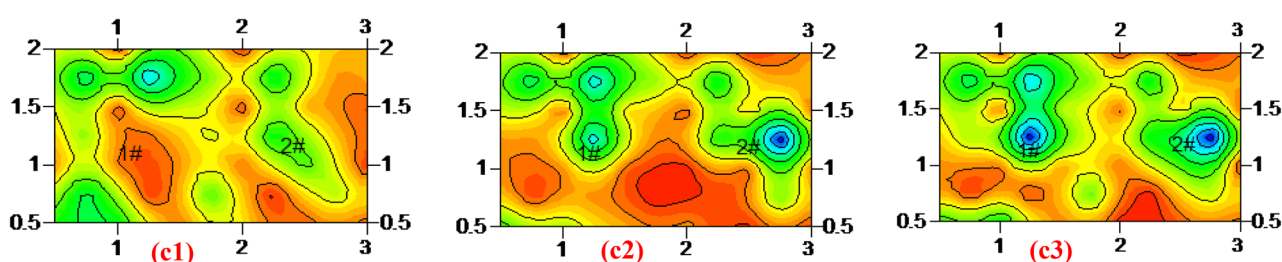
Unit: dm



(2) Fracture Y_{1-2} test results.



(3) Fracture Y_{1-3} test results.



(4) Fracture Y_{1-4} test results.

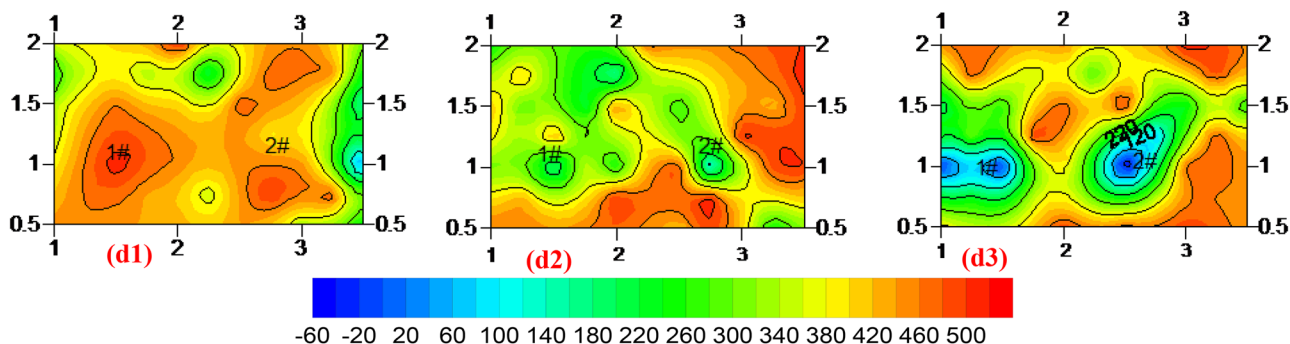
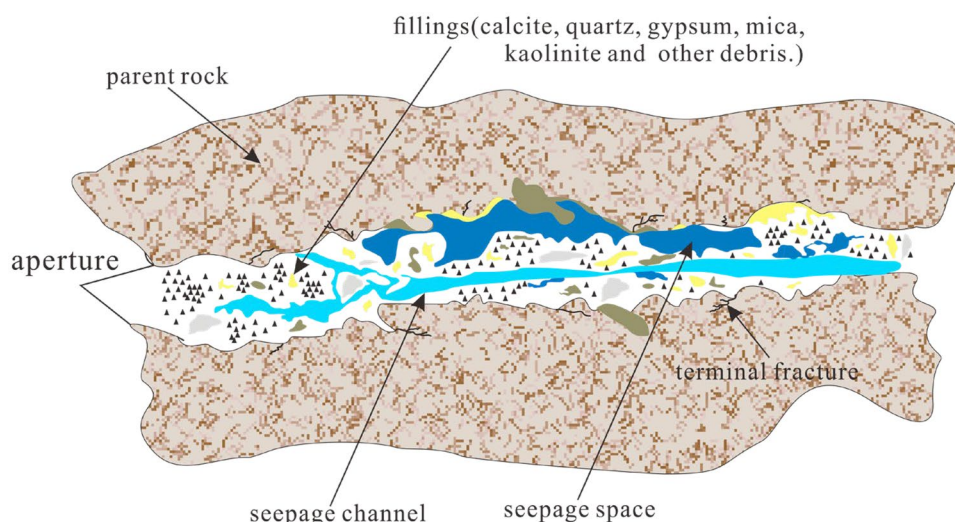


Fig. 12 Inversion results of geophysical electric method for four groups of typical fracture seepage. (a) The inversion result of fracture Y_{1-1} , in which (a1) is for the initial test (without adding any salt

water), (a2) is for the intermediate process test (adding 300 ml of salt water), and (a3) is for the last test (adding 500 ml of salt water). For other sets of experimental results, the same explanation is followed

Fig. 13 Geometric form of fracture aperture and its hydraulic conductivity



while the resistivity in the area between the two electrodes increased, which indicates that the salt water added to hole 2# converged to hole 1# along the fracture (Fig. 12a3). This suggests that fracture Y_{1-1} has good water conductivity, which is consistent with the fact that the fracture belongs to the open-weak filling type. Therefore, this type of fracture often plays an important role in the fracture network of a rock mass.

For fracture Y_{1-2} with two intersecting fractures (Figs. 2 and 8b), the inversion results reveal that the resistivity of the fracture zone decreased with the increase of the number of saline additions (Fig. 12b1, b2 and b3). This indicates that this group of fractures has a certain permeability, but the permeability is weaker than that of fracture Y_{1-1} .





Figure 12c shows that the entire experimental process only changed the resistivity of a small area around the electrode, while the resistivity in the area between the two electrodes barely changed. This also demonstrates that the fully cemented-closed type granite fractures (fracture Y_{1-3}) can be considered as not having conductivity in rock masses. However, this type of fracture is easily affected by

weathering and forms a large “false opening” on the surface (Fig. 8c), which results in the misconception of good water conductivity.

Another type of typical fracture is the loose filling type (fracture Y_{1-4}), which is a main fracture accompanied by many small fractures to form a fracture bundle (Figs. 2 and 8d). The geophysical inversion results reveal that this type of fracture exhibits weak connectivity and seepage during the experiment (Fig. 12d), which are however slightly better compared with those of the fracture Y_{1-3} . Similarly, this type of fracture also has a large “false opening,” owing to the influence of weathering on the surface.

In summary, the geometric features of the fracture aperture and the water conductivity (seepage) properties of the rock mass are shown in Fig. 13. The filling characteristics of different types and the corresponding seepage properties are summarized in Table 3. These findings will provide an important reference to the microscopic investigation of different fracture types with different characteristics and to fracture modeling and simulation in the future.

Table 3 Description of fractures filling characteristics and seepage

Fracture number	Filling type	Seepage properties	Feature description	Fracture morphology
Y_{1-1}	Open-weak filling	good	play an important water-conducting role in fracture network	
Y_{1-2}	Open filling	normal	play a water-conducting role in fracture network	
Y_{1-3}	Fully filled cemented form	no	play a water-blocking role in fracture network	
Y_{1-4}	Loose filling	weak	play a weak seepage role in fracture network	

Discussion

The application of the presented methodology for single natural fracture in granite body allowed us to reach important results, in terms of both acquisition of the fracture aperture characteristics in an efficient and low-cost way and regarding the applicability of the ERT technique in detecting the connectivity and permeability of granite fractures.

The principle of the measuring ruler dispersion-tangent middle axis method proposed to measure the fracture aperture is simple; that is, the precise value of the aperture can be obtained by combining the scale value with the pixel of the fracture in the same photo. Remarkably, this method requires only a camera and a ruler with a scale to complete the field measurement while ensuring the accuracy of the measurement, which provides an efficient and convenient method for geological engineers to conduct field investigation and geological bodies logging. One of the major advantages of the method is that the measurement results cannot be directly affected by the quality of the photos captured during the measurement. Because the ruler placed is relative to the fracture and the value of the scale determines the opening value. In particular, the quality of the captured photos affects the minimum measurement accuracy. This is because the photo quality (namely pixels) determines the size of a unit pixel. In general, the length of the natural fracture is much larger than the aperture value and the contour of the fracture is very complex; therefore, calculating the fracture aperture based on the middle axis of the fracture has certain advantages. This is because the tangent middle axis can accurately capture the two boundary points of the corresponding the middle axis point, which is different from the current method for obtaining the granular geometric form, such as soil particles or rock particles. It should be noted that compared with high precision CT imaging, the digital measurement method proposed in this study is also limited by the minimum measurement accuracy, but it can meet the engineering needs for field aperture measurement. This is because, aperture with too small size has no significant influence on the overall seepage flow in fracture network. As a result, in practical engineering, we are more concerned over the fractures with larger opening (aperture) size.

The ERT technique is widely used to investigate the internal physical characteristics affected by liquid, which is the most significant advantage compared with other geophysical methods. Therefore, it is also the direct reason why we consider using this technique to explore the seepage properties of natural fracture. Inspired by a large number of previous studies on water-bearing characteristics in the detection medium, we employed the ERT technique to infer the water-conducting characteristics of the granite fractures by

adding highly conductive salt water to the fractures through real-time monitoring. Granite is a hard rock with high resistivity. Therefore, it is helpful to enhance the conductivity by continuously adding salt water into the granite fracture. If the fracture has a good connectivity, these conductive particles will migrate along the fracture, causing the change of resistivity in the detection area. This provides a way of thinking for the diagnosis of potential hazards caused by solute migration in fractured media in rock-related engineering, such as bedrock dam construction site and nuclear waste disposal construction site.

Aperture and seepage properties of natural fractures are the two most important indexes in fracture network simulation. In this study, the different types of single fracture aperture and permeability were investigated systematically. The findings can contribute to improving the reliability of fracture network simulation. In addition, this study only considered the geometric characteristics of the aperture of the fresh fracture surface, and did not give the inherent reasons for the increase in the degree of aperture of the fracture surface caused by different weathering grades. Additionally, the inherent difference between the characteristics of the weathered surface fractures and the characteristics of fresh fractures is not included in the scope of this paper. These are the work that is worth studying in the future.

Conclusions

An investigation of the aperture geometry characteristics and the seepage properties of single natural fractures was performed at a well-exposed granite fracture site in Beishan area of China. Digital image measurement technology was proposed to capture the geometric characteristics of the aperture of the fresh fracture exposed by removing the weathered surface. The ERT technique was employed to investigate the characteristics of water conductivity and connectivity of granite fractures in rock mass. Our study leads to the following principal conclusions:

- (1) The presented measuring ruler dispersion-tangent middle axis method has the advantages of high efficiency and convenience for obtaining the geometric characteristics of fracture aperture, which can greatly reduce the field work for geological engineers and provide a low-cost and time-efficient method for fracture logging in the field.
- (2) The ERT technique used to investigate the connectivity and water conductivity of fractures in hard rocks such as granite has good applicability. After adding the salt solution, the resistivity of the fracture with good hydraulic conductivity changes greatly, while the monitoring results of the fracture with poor seepage do not change significantly.

- (3) Through the study of a typical fracture aperture, it is found that the value of the aperture obeys the following distribution: normal distribution, gamma distribution, lognormal distribution, and the generalized extreme value distribution, in which the best distribution for this study section is generalized extreme value distribution.
- (4) The four different fracture types are revealed by removing the weathered surface: namely, open-weak filling, open filling, loose filling, and fully cemented-closed form. The ERT inversion results suggest that water conductivity and seepage properties decrease as the filling density increases. Especially for the fully cemented-closed fracture, the filling material is easy to be affected by weathering and forms a pseudo fracture with large surface opening, causing the misconception of good water conductivity. Therefore, the filling and cementation characteristics of fractures are highly encouraged to be considered in the simulation of fracture seepage.

Due to the difficulty of field investigation, this study did not explore a large number of fractures and only selected a few typical ones. These findings help to reveal the control mechanism of the flow and transport in the fractured media inside the rock mass, which provide an important reference for the research of fracture characteristics and fracture modeling. In future studies, more typical fracture samples will also be considered in combination with in-situ water pressure test and tracer test.

Funding The authors received support from the National Key Research and Development Project of High-level Radioactive Waste Disposal of China (No. [2012]491; No. [2015]297; No. [2020]194) and the Nanjing University Innovation Program for PhD candidate (CXJ21-47). This project also received support from the Beijing Research Institute of Uranium Geology.

References

- Ali H, Kurokawa H, Uesugi K (2014) Camera based precision measurement in improving measurement accuracy. *Measurement* 49:38–147
- Azimian A, Ajalloeian R (2015) Permeability and groutability appraisal of the Nargesi dam site in Iran based on the secondary permeability index, joint hydraulic aperture and Lugeon tests. *Bull Eng Geol Environ* 74:845–859
- Baek SH, Kim SS, Kwon JS, Um ES (2017) Ground penetrating radar for fracture mapping in underground hazardous waste disposal sites: a case study from an underground research tunnel, south Korea. *J Appl Geophys* 141:24–33
- Banerjee S, Chakraborti PC, Saha SK (2019) An automated methodology for grain segmentation and grain size measurement from optical micrographs. *Measurement* 140:142–150
- Basu A, Celestino TB, Bortolucci AA (2009) Evaluation of rock mechanical behaviors under uniaxial compression with reference to assessed weathering grades. *Rock Mech Rock Eng* 42:73–93
- Bellanova J, Calamita G, Giocoli A, Luongo R, Macchiato M et al (2018) Electrical resistivity imaging for the characterization of the Montaguto landslide (southern Italy). *Eng Geol* 243:272–281
- Bharti AK, Prakash A, Verma A, Singh KKK (2021) Assessment of hydrological condition in strata associated with old mine working during and post-monsoon using electrical resistivity tomography: a case study. *Bull Eng Geol Environ* 80:5159–5166
- Brown SR, Kranz RL, Bonner BP (1986) Correlation between the surfaces of natural rock joints. *Geophys Res Lett* 13:1430–1433
- Chen L, Wang J, Zong ZH, Liu J et al (2015) A new rock mass classification system QHLW for high-level radioactive waste disposal. *Eng Geol* 190:33–51
- Detwiler RL, Pringle SE, Glass RJ (1999) Measurement of fracture aperture fields using transmitted light: an evaluation of measurement errors and their influence on simulations of flow and transport through a single fracture. *Water Resour Res* 35:2605–2617
- Fernlund JMR (2005) Image analysis method for determining 3-D size distribution of coarse aggregates. *Bull Eng Geol Environ* 64:159–166
- Geet MV, Swennen R (2001) Quantitative 3D-fracture analysis by means of microfocus X-ray computer tomography (μ CT): an example from coal. *Geophys Res Lett* 28:3333–3336
- Gentier S, Billiaux L, Vliet L (1989) Laboratory testing of the voids of a fracture. *Rock Mech Rock Eng* 22:149–157
- Guo L, Li XZ, Zhou YY, Zhang YS (2015) Generation and verification of three-dimensional network of fractured rock masses stochastic discontinuities based on digitalization. *Environ Earth Sci* 73:7075–7088
- Hooker JN, Laubach SE, Marrett R (2013) Fracture-aperture size frequency, spatial distribution, and growth processes in strata-bounded and non-strata-bounded fractures, Cambrian Mesón Group, NW Argentina. *J Struct Geol* 54:54–71
- Hoorde MV, Hermans T, Dumont G, Nguyen F (2017) 3D electrical resistivity tomography of karstified formations using cross-line measurements. *Eng Geol* 220:123–132
- Huang N, Jiang YJ, Liu RC, Li B, Sugimoto S (2019) A novel three-dimensional discrete fracture network model for investigating the role of aperture heterogeneity on fluid flow through fractured rock masses. *Int J Rock Mech* 116:25–37
- Huo D, Pini R, Benson SM (2016) A calibration-free approach for measuring fracture aperture distributions using X-ray computed tomography. *Geosphere* 12:558–571
- Karimpouli S, Tahmasebi P, Ramandi HL, Mostaghimi P, Saadatfar M (2017) Stochastic modeling of coal fracture network by direct use of micro-computed tomography images. *Int J Coal Geol* 179:153–163
- Kemna A, Vanderborght J, Kulesa B, Vereecken H (2002) Imaging and characterisation of subsurface solute transport using electrical resistivity tomography (ERT) and equivalent transport models. *J Hydrol* 267:125–146
- Ketcham RA, Mote AS (2019) Accurate measurement of small features in X-ray CT data volumes, demonstrated using gold grain. *J Geophys Res, Solid Earth* 124:3508–3529
- Li G, Liu QW, Zhao SM, Qiao WT, Ren XL (2020) Automatic crack recognition for concrete bridges using a fully convolutional neural network and naive bayes data fusion based on a visual detection system. *Meas Sci Technol* 31:075403. <https://doi.org/10.1088/1361-6501/ab79c8>
- Liu Y, Wang Q, Chen JP, Han XD, Song SY, Ruan YK (2021) Investigation of geometrical representative elementary volumes based on sampling directions and fracture sets. *Bull Eng Geol Environ* 80:2171–2187
- Loke MH, Barker RD (1995) Least-squares deconvolution of apparent resistivity pseudosections. *Geophysics* 60:1682–1690

- Mazumder S, Wolf KHAA, Elewaut K, Ephraim R (2006) Application of X-ray computed tomography for analyzing cleat spacing and cleat aperture in coal samples. *Int J Coal Geol* 68:205–222
- Montero R, Menendez E, Victores JG (2017) Balaguer C (2017) Intelligent robotic system for autonomous crack detection and characterization in concrete tunnels. *IEEE International Conference on Autonomous Robot Systems and Competitions* 4:316–321
- Nijland N, Meijde M, Addink EA, Jong SMD (2010) Detection of soil moisture and vegetation water abstraction in a Mediterranean natural area using electrical resistivity tomography. *CATENA* 81:209–216
- Priest SD (1993) *Discontinuity analysis for rock engineering*. Chapman and Hall, London
- Ramandi HL, Armstrong RT, Mostaghimi P (2016) Micro-CT image calibration to improve fracture aperture measurement. *Nondestruct Test Eva* 6:4–13
- Ramandi HL, Mostaghimi P, Armstrong RT (2017) Digital rock analysis for accurate prediction of fractured media permeability. *J Hydrol* 554:817–826
- Ravindran AA, Mondal NC, Ramanujam N, Srinivasamoorthy K, Anbazhagan P (2016) Appraisal of groundwater resource in holocene soil deposits by resistivity, hydrochemical and granulomerial studies in the gulf of mannar coast from southern India. *Environ Earth Sci* 75:166. <https://doi.org/10.1007/s12665-015-4883-8>
- Renshaw CE, Dadakis JS, Brown SR (2000) Measuring fracture apertures: a comparison of methods. *Geophys Res Lett* 27:289–292
- Schlüter S, Sheppard A, Brown K, Wildenschild D (2014) Image processing of multiphase images obtained via X-ray microtomography: a review. *Water Resour Res* 50:3615–3639
- Singh HK, Basu A (2018) Evaluation of existing criteria in estimating shear strength of natural rock discontinuities. *Eng Geol* 232:171–181
- Wang J (2010) High-level radioactive waste disposal in China: update 2010. *J Rock Mech Geotech* 2:1–11
- Wang J, Chen L, Su R, Zhang XG (2018) The beishan underground research laboratory for geological disposal of high-level radioactive waste in china: planning, site selection, site characterization and in situ tests. *J Rock Mech Geotech* 10:411–435
- Wang W (2006) Image analysis of particles by modified Ferret method—best-fit rectangle. *Powder Technol* 165:1–10
- Wu Y, Huang Z, Zhao K, Zeng W, Gu Q, Zhang R (2020) Unsteady seepage solutions for hydraulic fracturing around vertical wellbores in hydrocarbon reservoirs. *Int J Hydrog Energy* 45:9496–9503
- Xiong XB, Li B, Jiang YJ, Koyama T, Zhang CH (2011) Experimental and numerical study of the geometrical and hydraulic characteristics of a single rock fracture during shear. *Int J Rock Mech Min* 48:1292–1302
- Xu WT, Zhang YS, Li XZ, Wang XY et al (2021) Comprehensive identification of statistical homogeneity of fractured rock masses for a candidate HLW repository site, China. *Eng Geol* 293:106279. <https://doi.org/10.1016/j.enggeo.2021.106279>
- Xu WT, Zhang YS, Li XZ, Wang XY et al (2020) Extraction and statistics of discontinuity orientation and trace length from typical fractured rock mass: A case study of the Xinchang underground research laboratory site, China. *Eng Geol* 269:105553. <https://doi.org/10.1016/j.enggeo.2020.105553>
- Xu WT, Zhang YS, Li XZ, Wang XY, Zhang PX (2019) Study on three-dimensional fracture network connectivity path of rock mass and seepage characteristics based on equivalent pipe network. *Environ Earth Sci* 78:516. <https://doi.org/10.1007/s12665-019-8505-8>
- Yasuhara H, Polak A, Mitani Y, Grader AS, Halleck PM, Elsworth D (2006) Evolution of fracture seepage through fluid–rock reaction under hydrothermal conditions. *Earth Planet Sci Lett* 244:186–200
- Yu SN, Jang JH, Han CS (2007) Auto inspection system using a mobile robot for detecting concrete cracks in a tunnel. *Automat Constr* 16:255–261
- Zhang PX, Li XZ, Huang Z, Zhang YS, Yao XH (2019) Influence of fault zone on the respect distance and margin for excavation: a case study of the F4 fault in the Jijicao rock block, China. *Bull Eng Geol Environ* 78:2653–2669
- Zhang QG, Ju Y, Gong WB, Zhang L, Sun HF (2015) Numerical simulations of seepage flow in rough single rock fractures. *Petroleum* 1:200–205
- Zhang ZL, Yang JG, Ding LH, Zhao YM (2012) Estimation of coal particle size distribution by image segmentation. *Int J Min Sci Techno* 5:130–135
- Zhou QY, Shimada J, Sato A (2001) Three-dimensional spatial and temporal monitoring of soil water content using electrical resistivity tomography. *Water Resour Res* 37:273–285